Enhanced Acetone Sensing Based on Group-11 Metal (Cu, Ag, and Au) Nanoparticles Embedded in Graphitic Carbon Nitride (gCN)

Nihal [1,2,*], Rahul Sharma [1,2], Navjot Kaur [3], Mamta Sharma [1,*], B. C. Choudhary [3] and J. K. Goswamy [1]

1   Department of Applied Sciences, UIET, Panjab University, Chandigarh 160014, India
2   Centre for Nanoscience and Nanotechnology, Panjab University, Chandigarh 160014, India
3   Department of Applied Science, NITTTR, Chandigarh 160019, India
*   Correspondence: nihal.90414@gmail.com (N.); mamta.phys@gmail.com (M.S.)

Abstract: In this work, a group-11 metal nanoparticle-embedded, graphitic carbon nitride-based, resistive-type sensor was developed for room temperature acetone sensing. We synthesized pure and group-11 transition metal (Cu, Ag and Au) nanoparticles embedded in graphitic carbon nitride (gCN) by thermal polycondensation and chemical reduction methods. The synthesized material was characterized using UV/visspectroscopy, FTIRspectroscopy, XRD, HRTEM, FESEM, and EDS techniques. Sensing properties such as response, response/recovery time, selectivity, and stability were calculated. This study confirms that Ag/gCN is the best material for room temperature sensing of acetone compared to Cu/gCN, Au/gCN, and pure gCN. The response of Ag/gCN for 20 ppm acetone at room temperature is 28%. The response/recovery time is 42.05/37.09 s. Moreover, the response of Ag/gCN is stable for 10 days.

Keywords: acetone; gCN; sensing; transition metals; VOCs

1. Introduction

Acetone is a flammable and hazardous gas used as a solvent in producing rubber, fibers, and explosives [1,2]. In industries, when the acetone concentration reaches 300–500 ppm, it causes health hazards such as respiratory disorders and ocular irritation [3,4]. It also causes cardiovascular, urinary and digestive diseases [5]. Moreover, acetone is classified as a carcinogen by the US Environmental Protection Agency [6], and it also causes infertility in male as well as female animals [7]. Acetone can also act as a breath marker for the noninvasive and rapid detection of diabetes [8,9]. Thus, the detection of acetone is vital from a health and safety point of view. Several methods to detect gas include mass spectrometry, gas chromatography, differential mobility spectrometry and ion mobility spectrometry [10–14], but these techniques require sophisticated equipment, have high operational cost, and are time-consuming [15]. These limitations can be overcome by replacing these delicate techniques with nanomaterial-based sensing systems that are fast, portable, and low-cost [16].

Research on 2D nanomaterial has been gaining interest since the invention of graphene. Their extraordinary properties, such as excellent flexibility, greater mechanical strength, and high transparency, make 2D materials an appropriate candidate for sensing applications. Moreover, 2D materials with a single layer or a few layers exhibit quantum confinement, making them superior to bulk material. Graphitic carbon nitride (gCN) is one such 2D material that has attracted researchers for the last two decades due to its excellent nano-electronics and optoelectronic properties [17–22]. gCN is the most stable phase of carbon nitride, having tetrahedrally arranged carbon and nitrogen with several hybridizations (sp, sp^2 and sp^3) [23]. gCN contains polymeric defects that act as active sites for the adsorption of gas molecules. Cao et al. reported an ethanol sensor based on ZnO-decorated gCN

with a response of 15.8 towards 100 ppm of ethanol [24]. Zhang et al. also showed that a graphene–gCN nanocomposite possessed better sensing properties towards NO_2 gas than pure components [25]. Similarly, Meng et al. reported a ternary nanocomposite based on ZnO/GO/gCN for ethanol sensing, which showeda response of 178 for 100 ppm at 300 °C [26]. However, gCN has the drawback of electrical conductivity [22] and low adsorption performance [27]. Hence, some improvement in gCN toward sensing is required, which can be achieved by surface modification and doping. Various research has been going on to develop an efficient gCN-based sensing system through the decoration and doping of pristine gCN with metal or nonmetal atoms [28–32]. Incorporating transition metals such as Ag [33], Au [34] into gCN can overcome the drawbacks. The incorporation of transition metals into gCN can trap the electrons, thus prolonging the electron-hole recombination rate, making electrons available on the surface to interact more efficiently with the analyte [35]. Moreover, the localized surface plasmon resonance due to these noble metals can further support the interaction process between the sensor material and the analyte [8]. The electrical conductivity can also be enhanced by incorporating the transition metals in gCN, making it an efficient sensing material near room temperature [9].

Therefore, in the present study, weaimed to enhance the acetone-sensing properties of pure gCN by incorporating group-11 transition metal (Cu, Ag and Au) nanoparticles. This study shows that Ag/gCN is the best material for room temperature sensing of acetone compared to Cu/gCN, Au/gCN and pure gCN. The response of Ag/gCN for 20 ppm acetone at room temperature is 28%. The response/recovery time is 42.05/37.09 s.

2. Experimental Details

2.1. Synthesis of Bulk gCN and gCN Nanosheets

The bulk graphitic carbon nitride was synthesized by thermal polycondensation of urea. In a typical synthesis, 10 g of urea wasplaced in an alumina crucible and covered with a lid. The crucible wasthen placed in a furnace and heated at 5 °C/min till the temperature reached 550 °C and keptat this temperature for 4 h. The obtained powder wasthen ground into powder using a mortar pestle. The nanosheets of gCN were obtained from bulk gCN by a chemical exfoliation route. In this process, 1 g of bulk gCN was mixed with 10 mL of H_2SO_4 acid and stirred for 24 h. After that, 100 mL of DI water wasslowly poured into the above mixture. While mixing the DI water, the temperature increases rapidly, changing the color from brownish to light yellow. To remove the unexfoliated gCN from exfoliated gCN, the obtained pale-yellow suspension of gCN is centrifuged at 5000 rpm for 10 min. Finally, the suspension is washed with DI water and methanol several times, followed by overnight drying at 60 °C. Aschematic of the synthesis process of gCN bulk and nanosheets is shown in Figure 1.
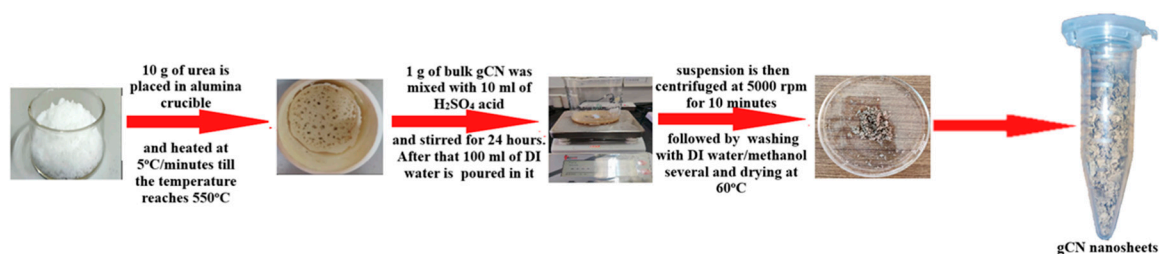

Figure 1. Schematic of synthesis process of gCN bulk and nanosheets.

2.2. Synthesis of Group-11 TM Nanoparticles Embedded gCN

Group-11 metal-embedded gCN was synthesized by chemical reduction of metal nanoparticles on gCN nanosheets. The metal salts used for Cu/gCN, Ag/gCN and Au/gCN synthesis were copper (II) chloride ($CuCl_2.2H_2O$), silver nitrate ($AgNO_3$) and chloroauric acid ($HAuCl_4$), respectively. Metal salt (5%) is mixed with pure gCN nanosheet aqueous solution (100 mg gCN in 100 mL DI water). The mixture solution is then sonicated using a probe sonicator for 10 min and then stirred for 30 min. After that, a fresh mixture

of 0.09 M NaOH and 0.04 M NaBH$_4$ is prepared. This solution is then poured into the metal salt mixture dropwise till the complete reduction of metal nanoparticles on gCN nanosheets is achieved. The obtained suspension is centrifuged and washed several times with DI water and ethanol. Finally, the suspension is dried at 60 °C for 6 h. A schematic of the synthesis process of group-11 metal-embedded gCN is shown in Figure 2.
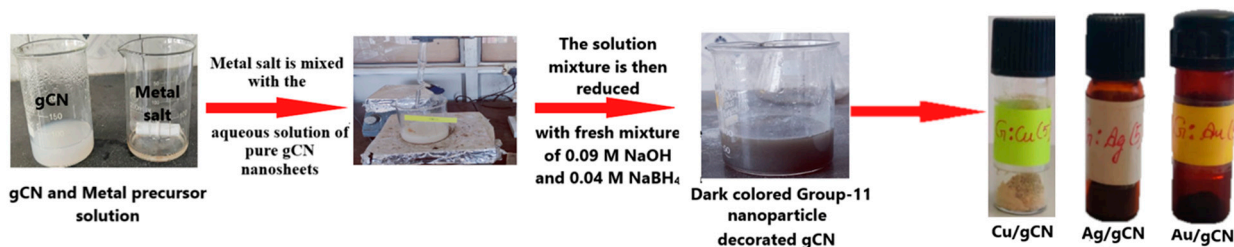

Figure 2. Schematic of synthesis process of group-11 metal-embedded gCN.

3. Material Characterizations

The prepared samples were characterized by UV/vis spectroscopy, FTIR, XRD, FESEM, EDS and HRTEM. UV/vis and FTIR characterization was performed using aShimadzuUV-2600 spectrometer and Shimadzu IRAffinity-1s, respectively. XRD characterization was performed using anX'Pert Pro diffractometer setup. FESEM and EDS analysis was performedusing aHitachi SU 8010. HRTEM was performedusing aJEOL 2100 Plus setup.

VOC sensing was performed using a stainless steel chamber of volume 1 L connected to asource meter (Agilent B2902A. The static volumetric method was adopted for the sensing study. A detailed schematic of the sensing setup is shown in Figure 3.
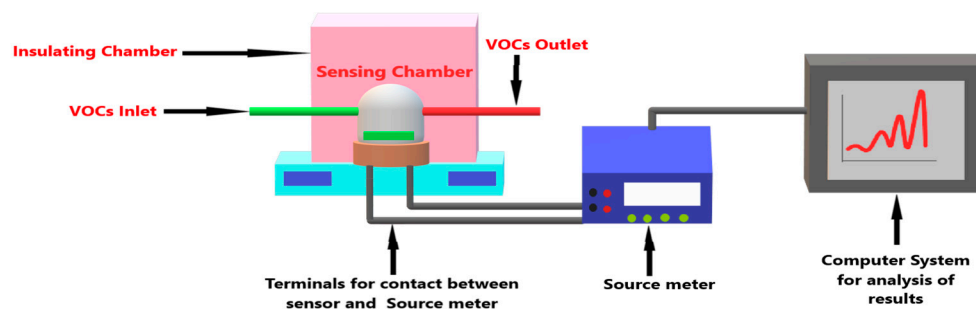

Figure 3. Schematic of sensing setup.

4. Results and Discussion

4.1. XRD

The XRD spectra of all the samples are shown in Figure 4. The XRD spectra of pure gCN and group-11 TM-embedded gCN were studied at diffraction angles in the range of 20–80 °C. For pure gCN, the presence of a distinct peak at 27.40° corresponds to the (002) plane, which is due to the interlayer and in-plan stacking of the triazine ring of gCN (JCPDS 87-1526) [36]. For Cu/gCN, two small peaks at 43.80° and 56.78° confirm the addition of Cu in gCN (Figures 3 and S2) [37]. These two peaks correspond to the (111) and (200) planes. For Ag/gCN, there are four extra peaks at 38.13°, 44.45°, 64.58° and 77.56°, which correspond to (111), (200), (220) and (311) planes of metallic Ag nanoparticles with cubic structure (JCPDS 65-2871) [36], whereas for Au/gCN, there exist extra peaks at 39.21°, 54.72° and 67.21° corresponding to (111), (200) and (220) planes. It can also be seen from the XRD spectra that the intensity of the peak at 27.40° corresponding to the gCN nanosheets remains almost identical in Cu/gCN, attributed to poor mixing of Cu nanoparticles with gCN such that that the Cu^{2+} ion does not change the skeleton structure of pure gCN [38], whereas the intensity of this peak is minimal in the case of Ag/gCN, confirming its excellent intermixing with gCN nanosheets compared to other samples. This excellent intermixing

of Ag with gCN is due to the Ag nanoparticles beinghighly stable compared to Cu and Au nanoparticles, which becomeagglomerated, resulting in poor intermixing.
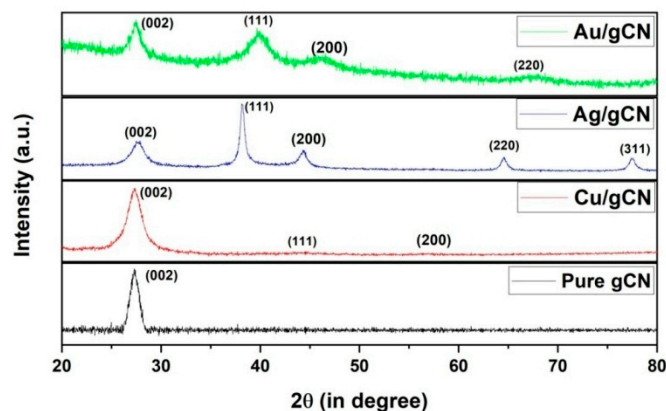

Figure 4. XRD spectra of pure gCN, Cu/gCN, Ag/gCN and Au/gCN.

4.2. UV/Vis Spectroscopy

The UV/vis spectra of pure gCN and group-11 metal (Cu, Ag and Au)-embedded gCN are shown in Figures 5 and 6, respectively. The Tauc relation is used to investigate the band gap (E_g):

$$\alpha h\upsilon = A\left(h\upsilon - E_g\right)^n \tag{1}$$

where $\alpha h\upsilon$ is the photon energy, E_g is the band gap, $n = 1/2$ for direct bandgap transition and A is constant which is different for different transitions
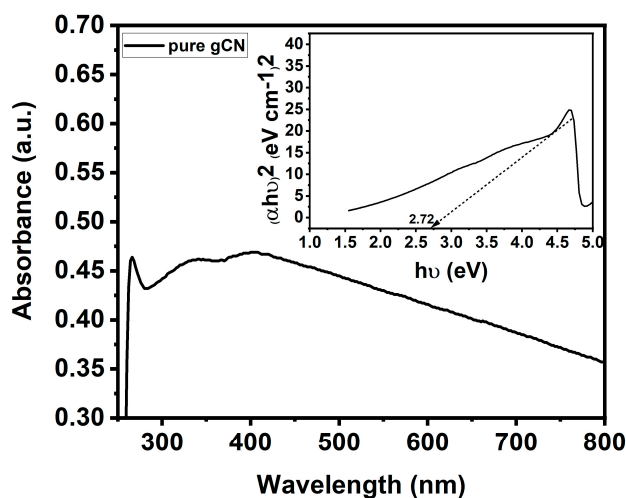

Figure 5. UV/vis spectra of pure gCN.

The Tauc plots of all materials areshown in the insets of UV/vis spectra (Figures 4 and 5). By extrapolating the tangent of $(\alpha h\upsilon)^2$ on the $h\upsilon$ axis, the band gap is calculated for all the materials. For pure gCN, the calculated band gap was 2.72 eV, which matches well with the literature [39]. For Cu/gCN, Ag/gCN and Au/gCN, the bandgap decreases to 2.63, 1.39 and 1.71 eV, respectively. This decrease in bandgap is due to the incorporation of metallic nanoparticles in metal-free gCN. Since gCN is a metal-free semiconductor, it has poor electrical conductivity, but with the addition of metal nanoparticles in it, the bandgap decreases since the material changes from a semiconducting nature to a conducting nature. Of all the materials, Ag/gCN has the lowest band gap, which confirms that of all three metal nanoparticles, Ag nanoparticles have the best affinity with pure gCN, followed by Au/gCN, whereas for Cu/gCN, there is the least change in bandgap value (2.63 eV) compared to pure gCN (2.72 eV), which confirms its poor interaction with pure gCN.
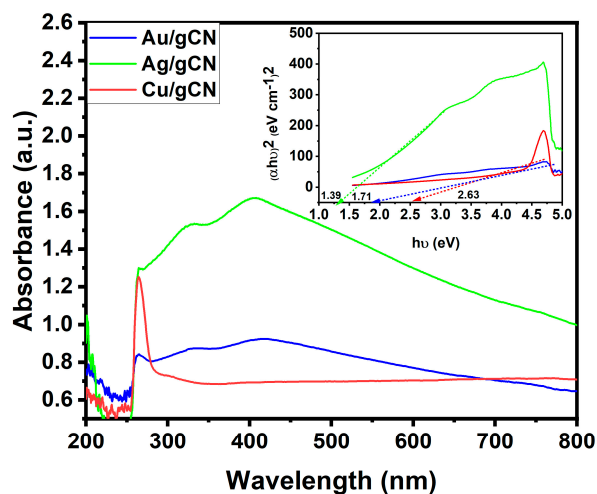
Figure 6. UV/vis spectra of Cu/gCN, Ag/gCNand Au/gCN.

4.3. FTIR Spectroscopy

The FTIR spectra of pure and group-11 TM nanoparticle-embedded gCN is shown in Figure 7. FTIR spectra are studied to analyze the molecular structure of gCN and its nanocomposite. A wide adsorption band observed in a range of 3000–3400 cm^{-1} is partially due to the terminal NH_2 and NH groups of the gCN surface and partially due to the OH group of surface-adsorbed water molecules [40,41]. The multiple peaks in the range of 1200–1650 cm^{-1} are due to the stretching vibration modes of C=N and C-N in the heterocyclic aromatic rings [42]. Moreover, the peak at 812 cm^{-1} is attributed to the stretching vibration mode of the triazine monomer of gCN [43]. The FTIR spectra of Cu, Ag and Au embedded gCN have similar peaks as that of pure gCN. Thus,the FTIR study shows that the addition of group-11 metal nanoparticles does not alter the molecular structure of pure gCN.
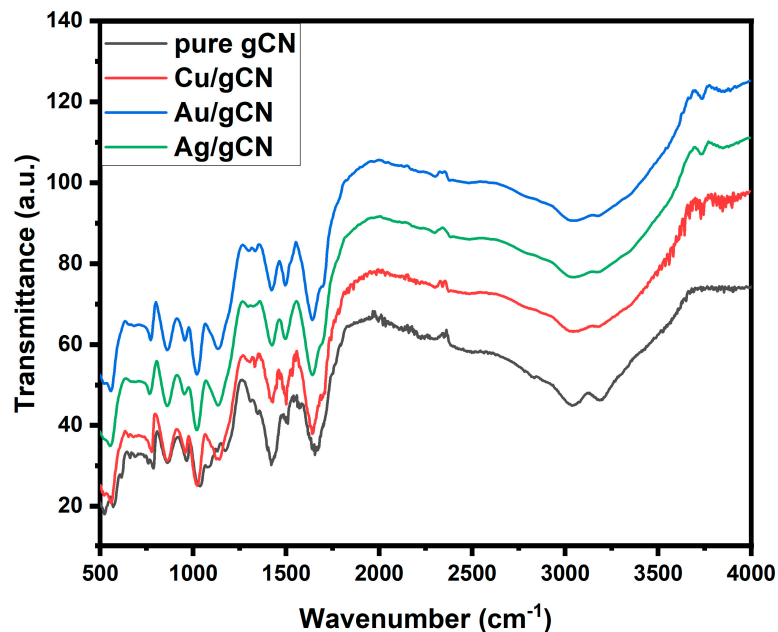

Figure 7. FTIR spectra of pure gCN and Cu-, Ag-, and Au-embedded gCN.

4.4. FESEM and EDS

The surface morphology and elemental analysis of pure gCN and group-11 TM nanoparticle-embedded gCN were studied using FESEM and EDS and elemental mapping. FESEM image of pure gCN is shown in Figure 8a. It can be seen that pure gCN shows a sheet-like structure witha coarse surface. EDS and elemental mapping show 39.77 and 69.23 wt% of C and N, respectively (Figure S3). For Cu/gCN (Figure 8b), the FESEM image shows that the surface of gCN becomes rougher and coarser after Cu decoration. EDS and elemental mapping show 36.72%, 56.92% and 6.36% of C, N and Cu in Cu/gCN (Figure S4). For Ag/gCN (Figure 8c) and Au/gCN (Figure 8d), adding Ag and Au changes the surface of pure gCN with more irregularity and roughness than Cu/gCN and pure gCN. The EDS spectra confirm that 6.06 wt% of Ag and 4.15% of Au is added in Ag/gCN (Figure S5) and Au/gCN (Figure S6), respectively. The maximum change in surface morphology can be observed for Ag/gCN because the addition of Ag in gCN is an energetically favorable process compared to Cu and Au addition.
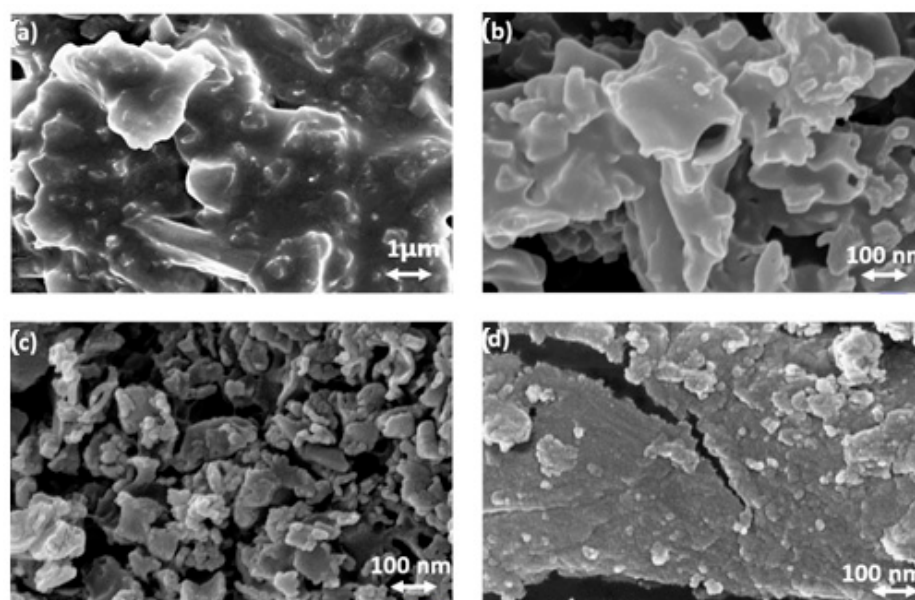

Figure 8. FESEM images of (**a**) pure gCN; (**b**) Cu/gCN; (**c**) Ag/gCN; (**d**) Au/gCN.

4.5. HRTEM

HRTEM analysis is also done on pure and group-11 TM nanoparticle-embedded gCN to understand more about the morphology of all the samples. Figure 9 shows HRTEM images of pure gCN and Cu-, Ag-, and Au-embedded gCN. For pure gCN, a smooth morphology with voids can be observed. These voids are due to the acidic exfoliation of bulk gCN into gCN nanosheets. Compared to Ag and Au embedded gCN, very few Cu nanoparticles in Cu/gCN can be seen, which confirms the less intense peaks of the XRD pattern of Cu/gCN (Figure 4). Agglomeration of Au nanoparticles can be observed in Au/gCN, resulting in a greater size of Au nanoparticles on the gCN sheet, whereas a uniform dispersion of Ag nanoparticles of size 7–10 nm on gCN nanosheets can be seen, whichfurther proves the better addition of Ag in gCN than Cu and Au.
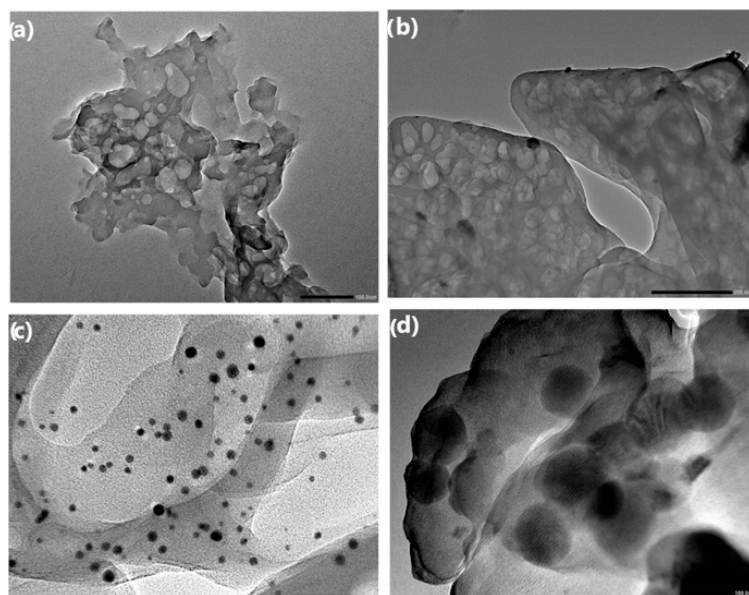
Figure 9. HRTEM images: (**a**) gCN nanosheets; (**b**) Cu/gCN; (**c**) Ag/gCN; (**d**) Au/gCN.

4.6. Sensing

The VOC sensing study was performed in a 1 L sensing chamber made of stainless steel connected to a source meter (Agilent B2902A) with two terminals. The static volumetric method was used for all the measurements.

For calculating the volume of target VOC, the following formula was used:

$$C = \frac{22.4 \times \varphi \times \rho \times V_1}{M \times V_2} \tag{2}$$

where

C is the concentration of analyte in ppm,
φ is the volume fraction of gas,
ρ is the density of the analyte in g/mL,
V_1 is the volume of analyte in μL,
V_2 is the volume of the sensing chamber in L, and
M is the molecular mass of the analyte in g/mol.

The sensor response was calculated using Equation (3) (for pure gCN) and Equation (4) (for group-11 TM-embedded gCN) [44,45]:

$$Response(\%) = \frac{R_{VOC} - R_A}{R_{VOC}} \tag{3}$$

and

$$Response(\%) = \frac{R_A - R_{VOC}}{R_A} \tag{4}$$

where R_{VOC} is the resistance of sensing material in the presence of VOC vapors, and R_A is the resistance of sensing material in the absence of VOC.

The sensing response of all the materials was assessedat room temperature with a relative humidity of ~45%. The concentration range of acetone exposure was in the range of 20–100 ppm. For pure gCN, the response shows an upward trend. However, in comparison to pure gCN, group-11 TM metal nanoparticle (Cu, Ag and Au)-embedded gCN exhibits a response curve of the opposite pattern. This shows that pure gCN shows a p-type response to ammonia, whereas Cu/gCN, Ag/gCN and Au/gCN show n-type behavior towards acetone sensing.

The acetone-sensing study was performed at room temperature using a stainlesssteel chamber of 1 L volume with a two-terminal source meter. The static volumetric method was used [46].

The response curves of pure gCN nanosheets are shown in Figure S1 (Supplementary Data), and those of Cu/gCN, Ag/gCN and Au/gCN are shown in Figure 10a–c. For 20 ppm of acetone, the response of pristine gCN is 6%, which increases to 25%, 28% and 24% for Cu/gCN, Ag/gCN and Au/gCN, respectively. For 100 ppm of acetone, the response of pure gCN is 35% only, which is enhancedto 66%, 79% and 65% for Cu/gCN, Ag/gCN, and Au/gCN, respectively. Hence, we can see the response increase with the addition of transition metal in gCN, with a maximum response for Ag/gCN, followed by Cu/gCN and Au/gCN.
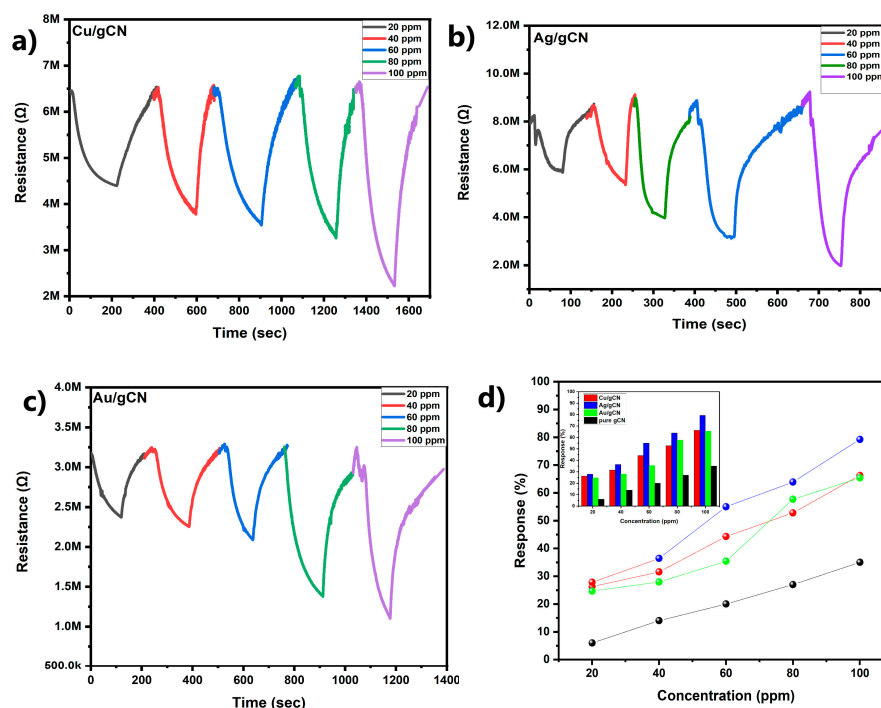

Figure 10. Sensing response of (**a**) Cu/gCN (**b**) Ag/gCN and (**c**) Au/gCN; (**d**) variation inresponse with concentration of acetone.

The response/recovery time wasalso calculated for all the samples. Response time is the time taken by the sensor to reach 90% of maximum value of its response in the presence of analyte, whereas recovery time is the time taken by a sensor to recover 90% of the maximum value of its response after the analyte is removed. The response time for 20 ppm exposure of acetone was 103.00, 125.94, 42.05 and 71.82 s for pristine gCN, Cu/gCN, Ag/gCN and Au/gCN, respectively. The recovery time was 94.21, 154.65, 37.09 and 65.75 s for pristine gCN, Cu/gCN, Ag/gCN and Au/gCN, respectively. Hence, the response and recovery time were the shortest for Ag/gCN out of all the materials, which further confirms that Ag-embedded gCN is the best material for acetone sensing among all the materials under study.

The response variation based on acetone concentration is shown in Figure 10d. The inset of Figure 10d shows a bar graph of response vs concentration of acetone. We can see that the response increases with an increase in the acetone concentration (20 to 100 ppm). Thus, all the materials show linear response with an increase in the concentration of acetone.

The selectivity and stability of Ag/gCN are also investigated (Figure 11a,b, respectively). The selectivity was calculated using 20 ppm of methanol, propan-2-ol, toluene and cyclohexane as analytes. It can be seen from Figure 11a that Ag/gCN is the most sensitive for acetone (28%) of all five analytes. The response of Ag/gCN for 20 ppm

of methanol, propane-2-ol, toluene, and cyclohexane is 20%, 13.60%, 10.54% and 5.89%, respectively. The stability of Ag/gCN is calculated by performing the acetone sensing under similar conditions for 20 ppm concentration for 10 days. It can be seen from the stability curve (Figure 11b) that the response remains almost the same for 10 days. Hence, Ag/gCN is a commendable material in terms of response, response/recovery time selectivity, and stability.
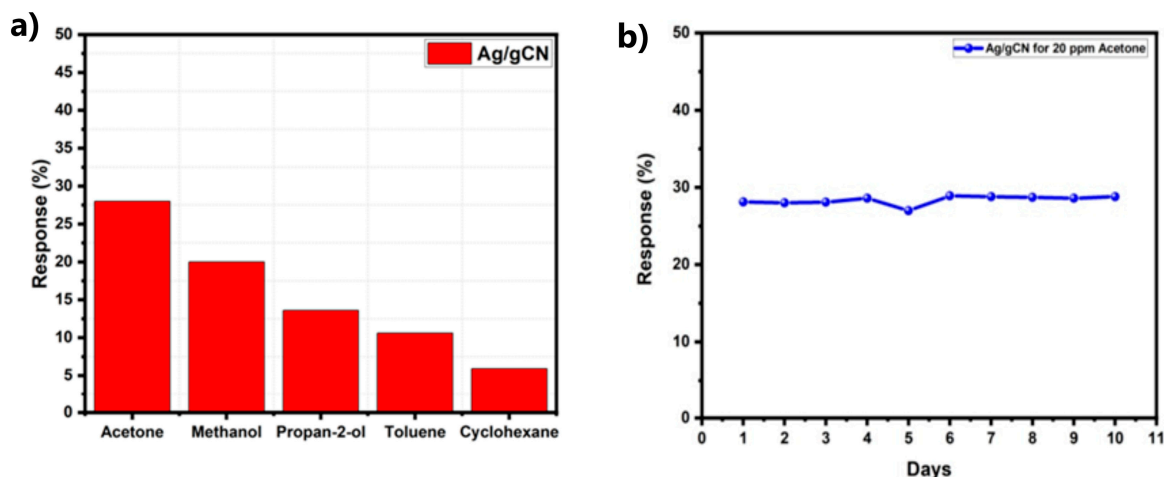
a)

b)

Figure 11. (**a**) Selectivity of Ag/gCN towards various VOCs; (**b**) stability of Ag/gCN for acetone sensing.

4.7. Sensing Mechanism

Our study depicts that Ag/gCN is the best material for acetone-sensing compared to pristine gCN, Cu/gCN and Au/gCN. Thus, the sensing mechanism of Ag/gCN is discussed in this section.

The sensing mechanism of Ag/gCN is based on the interaction of acetone molecules with Ag nanoparticles on the sensor surface [47,48] The conversion of Ag into AgO occurs when acetone molecules interact with Ag nanoparticles. This interaction results in a decrease in the work function of the acetone molecule over the surface of Ag/gCN. The free electrons of acetone molecules thus drift towards the gCN surface and get impregnated on the gCN lattice [49]. This will result in an increase in charge carrier concentration in Ag/gCN, which leads to an increase in conductance and therefore a decrease in resistance of Ag/gCN. This decrease in resistance is the reason behind the n-type behavior of Ag/gCN towards acetone sensing. The resistance increases when the acetone molecule desorbs from the surface of Ag/gCN, since the resistance of the sensor depends upon the concentration of the analyte [49].

Ag/gCNalso acts as an n-type semiconducting sensor [50]. When it is exposed toair, the adsorbed oxygen from the surrounding atmosphere becomesionized to O_2^-, O^-, and O^{2-} by accepting electrons from conduction band. This results in the formation of a thick depletion layer and thus increases the width of the potential barrier. This will increase the resistance of the sensor [51]. When Ag/gCN is exposed to acetone, which is reducing in nature, the already-adsorbed oxygen species come in contact with it [52]. This interaction results in the release of trapped electrons back to the conduction band, which will decrease the resistance of the sensor. Thus, the redox reaction between the acetone and adsorbed oxygen further enhances the sensing response.

Thus, we can say that in the present study, compared to pure gCN, Cu/gCN, and Au/gCN, Ag/gCN has superior sensing properties towards acetone vapors at room temperature (Table 1). For 20 ppm of acetone, the response of Ag/gCN six times that of pure gCN. The response and recovery time also reduces to 2.4 and 2.5 times, respectively. Moreover, Ag/gCN is highly selective compared to other materials, with good stability for 10 days.

Table 1. Comparison of different gCN-based sensors with the present study.

Sr.No.	Material	Analyte	Response (%)	Operating Temperature (°C)	Reference
1.	Exfoliated polymeric carbon nitride	Ethanol	2.31	20 ± 2°	[53]
2.	$Pd/SnO_2/g$-C_3N_4	CO	5.55	125	[54]
3.	In(III)-SnO_2/g-CN	Toluene	2.4	90	[55]
4.	Pure gCN Ag/gCN	Ethanol	6.67 14.87	Room temperature	[56]
5.	Cu/gCN Ag/gCN Au/gCN	Acetone	25 28 24	Room Temperature	This work

5. Conclusions

In this study, pure and group-11 transition metals (Cu, Ag,and Au) were embedded graphitic carbon nitride (gCN) by thermal polycondensation and chemical reduction for sensing acetone. The experimental characterization confirmed the successful synthesis of pure and transition metal-embedded gCN. The response for 20 ppm acetone was 6%, 25%, 28% and 24% for pure gCN, Cu/gCN, Ag/gCN and Au/gCN, respectively. The response and recovery time wasalso the least for Ag/gCN, i.e., 42.05 and 37.09 s. Further, good linearity was observed for response with the variation inconcentration of acetone for all the materials. Finally, the stability and selectivity were also studied for Ag/gCN, which also confirms the aptness of this material for acetone sensing. Thus, our study suggests that the addition of group-11 transition metalstopristine gCN enhances its sensing properties.

Supplementary Materials: The following supporting information can be downloaded at https://www.mdpi.com/article/10.3390/atoms11050078/s1. Figure S1: Sensing Response of pure gCN, Figure S2: Detailed XRD spectra of Cu/gCN, Figure S3: EDS and mapping or pure gCN, Figure S4: EDS and mapping or Cu/gCN, Figure S5: EDS and mapping or Ag/gCN, Figure S6: EDS and mapping or Au/gCN.

Author Contributions: N. performed the investigation, experimentation and write the original draft. R.S. helped in experimentation. N.K. contributed to data validation and characterization. M.S. curated the data and involved in supervision. B.C.C. was involved in conceptualization, editing and supervision. J.K.G. involved in supervision, conceptualization and editing. All authors have read and agreed to the published version of the manuscript.

Data Availability Statement: Data is contained within the article or supplementary material.

Conflicts of Interest: The authors declare no conflict of interest.

References

1. Liew, F.E.; Nogle, R.; Abdalla, T.; Rasor, B.J.; Canter, C.; Jensen, R.O.; Wang, L.; Strutz, J.; Chirania, P.; de Tissera, S.; et al. Carbon-negative production of acetone and isopropanol by gas fermentation at industrial pilot scale. *Nat. Biotechnol.* **2022**, *40*, 335–344. [CrossRef] [PubMed]
2. Weber, I.C.; Braun, H.P.; Krumeich, F.; Güntner, A.T.; Pratsinis, S.E. Superior Acetone Selectivity in Gas Mixtures by Catalyst-Filtered Chemoresistive Sensors. *Adv. Sci.* **2020**, *7*, 2001503. [CrossRef]
3. Chang, H.; Motagamwala, A.H.; Huber, G.W.; Dumesic, J.A. Synthesis of biomass-derived feedstocks for the polymers and fuels industries from 5-(hydroxymethyl)furfural (HMF) and acetone. *Green Chem.* **2019**, *21*, 5532–5540. [CrossRef]
4. Singh, M.; Kaur, N.; Drera, G.; Casotto, A.; Sangaletti, L.; Comini, E. SAM Functionalized ZnO Nanowires for Selective Acetone Detection: Optimized Surface Specific Interaction Using APTMS and GLYMO Monolayers. *Adv. Funct. Mater.* **2020**, *30*, 2003217. [CrossRef]

5. Available online: https://naturalpedia.com/acetone-toxicity-side-effects-diseases-and-environmental-impacts.html (accessed on 15 February 2023).

6. US Environmental Protection Agency (EPA), Integrated Risk Information System (IRIS). Summary on Acetone (67-64-1). 2000. Available online: http://www.epa.gov/iris (accessed on 17 January 2014).

7. New Jersey Department of Health and Senior Services. Hazardous Substance Fact Sheet for Acetone. 2014. Available online: http://nj.gov/health/eoh/rtkweb/documents/fs/0006.pdf (accessed on 25 January 2014).

8. Sharma, R.; Nihal Sharma, M.; Goswamy, J.K. Synthesis and characterization of MoS_2/WO_3 nanocomposite for electrochromic device application. *Int. J. Energy Res.* **2022**, *46*, 22176–22187. [CrossRef]

9. Sharma, R.; Nihal Sharma, M.; Goswamy, J.K. $LiMn_2O_4$ -rGO/PANI Nanocomposite as a Cathode Material for Li-Ion Batteries. *J. Electrochem. Soc.* **2022**, *169*, 083505. [CrossRef]

10. Zhou, X.; Zou, Y.; Ma, J.; Cheng, X.; Li, Y.; Deng, Y.; Zhao, D. Cementing Mesoporous ZnO with Silica for Controllable and Switchable Gas Sensing Selectivity. *Chem. Mater.* **2019**, *31*, 8112–8120. [CrossRef]

11. Wang, R.; Lan, K.; Chen, Z.; Zhang, X.; Hung, C.-T.; Zhang, W.; Wang, C.; Wang, S.; Chen, A.; Li, W.; et al. Janus Mesoporous Sensor Devices for Simultaneous Multivariable Gases Detection. *Matter* **2019**, *1*, 1274–1284. [CrossRef]

12. Afreen, S.; Zhu, J.-J. Rethinking EBAD: Evolution of smart noninvasive detection of diabetes. *TrAC Trends Anal. Chem.* **2019**, *118*, 477–487. [CrossRef]

13. Fang, C.-J.; You, H.-C.; Huang, Z.-L.; Hsu, C.-L.; Tsai, C.-F.; Lin, Y.-T.; Kao, Y.-M.; Tseng, S.-H.; Wang, D.-Y.; Su, N.-W. Simultaneous Analysis of the Stable Carbon Isotope Ratios of Acetoin and Acetic Acid by GC-C-IRMS for Adulteration Detection in Brewed Rice Vinegar Products. *J. Agric. Food Chem.* **2020**, *68*, 14252–14260. [CrossRef]

14. Siebert, L.; Wolff, N.; Ababii, N.; Terasa, M.-I.; Lupan, O.; Vahl, A.; Duppel, V.; Qiu, H.; Tienken, M.; Mirabelli, M.; et al. Facile fabrication of semiconducting oxide nanostructures by direct ink writing of readily available metal microparticles and their application as low power acetone gas sensors. *Nano Energy* **2020**, *70*, 104420. [CrossRef]

15. Cao, C.; Yuan, Q.; Wang, C.; Deng, L.; Li, H.; Wang, D. Controlled synthesis of hierarchical tungsten oxide hydrates for efficient acetone detection. *Appl. Surf. Sci.* **2022**, *604*, 154651. [CrossRef]

16. Nihal Sharma, R.; Kaur, N.; Choudhary, B.C.; Goswamy, J.K. DFT based study of transition metals (Au, Ag, Pd & Pt) doped graphitic carbon nitride (gCN) monolayer as a CO gas sensor. *Phys. Scr.* **2022**, *97*, 065706. [CrossRef]

17. Zhao, Z.; Sun, Y.; Dong, F. Graphitic carbon nitride based nanocomposites: A review. *Nanoscale* **2015**, *7*, 15–37. [CrossRef]

18. Mamba, G.; Mishra, A.K. Graphitic carbon nitride (g-C 3 N 4) nanocomposites: A new and exciting generation of visible light driven photocatalysts for environmental pollution remediation. *Appl. Catal. B Environ.* **2016**, *198*, 347–377. [CrossRef]

19. Cao, S.; Low, J.; Yu, J.; Jaroniec, M. Polymeric Photocatalysts Based on Graphitic Carbon Nitride. *Adv. Mater.* **2015**, *27*, 2150–2176. [CrossRef] [PubMed]

20. Zhou, L.; Zhang, H.; Sun, H.; Liu, S.; Tade, M.O.; Wang, S.; Jin, W. Recent advances in non-metal modification of graphitic carbon nitride for photocatalysis: A historic review. *Catal. Sci. Technol.* **2016**, *6*, 7002–7023. [CrossRef]

21. Huang, D.; Yan, X.; Yan, M.; Zeng, G.; Zhou, C.; Wan, J.; Cheng, M.; Xue, W. Graphitic Carbon Nitride-Based Heterojunction Photoactive Nanocomposites: Applications and Mechanism Insight. *ACS Appl. Mater. Interfaces* **2018**, *10*, 21035–21055. [CrossRef]

22. Oseghe, E.O.; Akpotu, S.O.; Mombeshora, E.T.; Oladipo, A.O.; Ombaka, L.M.; Maria, B.B.; Idris, A.O.; Mamba, G.; Ndlwana, L.; Ayanda, O.S.; et al. Multi-dimensional applications of graphitic carbon nitride nanomaterials—A review. *J. Mol. Liq.* **2021**, *344*, 117820. [CrossRef]

23. Mousavi, M.; Habibi-Yangjeh, A.; Pouran, S.R. Review on magnetically separable graphitic carbon nitride-based nanocomposites as promising visible-light-driven photocatalysts. *J. Mater. Sci. Mater. Electron.* **2018**, *29*, 1719–1747. [CrossRef]

24. Cao, J.; Gong, Y.; Wang, Y.; Zhang, B.; Zhang, H.; Sun, G.; Bala, H.; Zhang, Z. Cocoon-like ZnO decorated graphitic carbon nitride nanocomposite: Hydrothermal synthesis and ethanol gas sensing application. *Mater. Lett.* **2017**, *198*, 76–80. [CrossRef]

25. Zhang, S.; Hang, N.; Zhang, Z.; Yue, H.; Yang, W. Preparation of g-C3N4/Graphene Composite for Detecting NO_2 at Room Temperature. *Nanomaterials* **2017**, *7*, 12. [CrossRef] [PubMed]

26. Meng, F.; Chang, Y.; Qin, W.; Yuan, Z.; Zhao, J.; Zhang, J.; Han, E.; Wang, S.; Yang, M.; Shen, Y.; et al. ZnO-Reduced Graphene Oxide Composites Sensitized with Graphitic Carbon Nitride Nanosheets for Ethanol Sensing. *ACS Appl. Nano Mater.* **2019**, *2*, 2734–2742. [CrossRef]

27. Nihal Sharma, R.; Kaur, N.; Choudhary, B.C.; Goswamy, J.K. DFT based comparative study of pristine gCN and gCN-ZnO composite as a sensor for CO and CO2 gases. *Mater. Lett.* **2022**, *324*, 132649. [CrossRef]

28. Wang, Y.; Wang, X.; Antonietti, M. Polymeric Graphitic Carbon Nitride as a Heterogeneous Organocatalyst: From Photochemistry to Multipurpose Catalysis to Sustainable Chemistry. *Angew. Int. Ed.* **2012**, *51*, 68–89. [CrossRef]

29. Zheng, Y.; Lin, L.; Wang, B.; Wang, X. Graphitic Carbon Nitride Polymers toward Sustainable Photoredox Catalysis. *Angew. Int. Ed.* **2015**, *54*, 12868–12884. [CrossRef]

30. Xu, B.; Ahmed, M.B.; Zhou, J.L.; Altaee, A.; Xu, G.; Wu, M. Graphitic carbon nitride based nanocomposites for the photocatalysis of organic contaminants under visible irradiation: Progress, limitations and future directions. *Sci. Total Environ.* **2018**, *633*, 546–559. [CrossRef]

31. Jiang, L.; Yuan, X.; Pan, Y.; Liang, J.; Zeng, G.; Wu, Z.; Wang, H. Doping of graphitic carbon nitride for photocatalysis: A reveiw. *Appl. Catal. B Environ.* **2017**, *217*, 388–406. [CrossRef]

32. Sun, Y.; Ha, W.; Chen, J.; Qi, H.; Shi, Y. Advances and applications of graphitic carbon nitride as sorbent in analytical chemistry for sample pretreatment: A review. *TrAC Trends Anal. Chem.* **2016**, *84*, 12–21. [CrossRef]

33. Leong, K.H.; Liu, S.L.; Sim, L.C.; Saravanan, P.; Jang, M.; Ibrahim, S. Surface reconstruction of titania with g-C3N4 and Ag for promoting efficient electrons migration and enhanced visible light photocatalysis. *Appl. Surf. Sci.* **2015**, *358*, 370–376. [CrossRef]

34. Zada, A.; Qu, Y.; Ali, S.; Sun, N.; Lu, H.; Yan, R.; Zhang, X.; Jing, L. Improved visible-light activities for degrading pollutants on TiO2/g-C3N4 nanocomposites by decorating SPR Au nanoparticles and 2,4-dichlorophenol decomposition path. *J. Hazard. Mater.* **2018**, *342*, 715–723. [CrossRef] [PubMed]

35. Hou, W.; Cronin, S.B. A Review of Surface Plasmon Resonance-Enhanced Photocatalysis. *Adv. Funct. Mater.* **2013**, *23*, 1612–1619. [CrossRef]

36. Veerakumar, P.; Rajkumar, C.; Chen, S.-M.; Thirumalraj, B.; Lin, K.-C. Ultrathin 2D graphitic carbon nitride nanosheets decorated with silver nanoparticles for electrochemical sensing of quercetin. *J. Electroanal. Chem.* **2018**, *826*, 207–216. [CrossRef]

37. Yuan, J.; Yang, M.-P.; Zhi, W.-Y.; Wang, H.; Wang, H.; Lu, J.-X. Efficient electrochemical reduction of CO2 to ethanol on Cu nanoparticles decorated on N-doped graphene oxide catalysts. *J. CO_2 Util.* **2019**, *33*, 452–460. [CrossRef]

38. Chen, Y.; Zhu, Y.; Zhao, Y.; Wang, J. Fluorescent and colorimetric dual-response sensor based on copper (II)-decorated graphitic carbon nitride nanosheets for detection of toxic organophosphorus. *Food Chem.* **2021**, *345*, 128560. [CrossRef]

39. Basharnavaz, H.; Habibi-Yangjeh, A.; Mousavi, M. Ni, Pd, and Pt-embedded graphitic carbon nitrides as excellent adsorbents for HCN removal: A DFT study. *Appl. Surf. Sci.* **2018**, *456*, 882–889. [CrossRef]

40. Han, J.; Zou, H.Y.; Liu, Z.X.; Yang, T.; Gao, M.X.; Huang, C.Z. Efficient visible-light photocatalytic heterojunctions formed by coupling plasmonic Cu_{2-x} Se and graphitic carbon nitride. *N. J. Chem.* **2015**, *39*, 6186–6192. [CrossRef]

41. Yao, Y.; Lu, F.; Zhu, Y.; Wei, F.; Liu, X.; Lian, C.; Wang, S. Magnetic core–shell CuFe2O4@C3N4 hybrids for visible light photocatalysis of Orange II. *J. Hazard. Mater.* **2015**, *297*, 224–233. [CrossRef]

42. Saravanakumar, K.; Mamba, G.; Muthuraj, V. 1D/2D MnWO4 nanorods anchored on g-C3N4 nanosheets for enhanced photocatalytic degradation ofloxacin under visible light irradiation. *Colloids Surf. A Physicochem. Eng. Asp.* **2019**, *581*, 123845. [CrossRef]

43. Li, H.; Jing, Y.; Ma, X.; Liu, T.; Yang, L.; Liu, B.; Yin, S.; Wei, Y.; Wang, Y. Construction of a well-dispersed Ag/graphene-like g-C$_3$N$_4$ photocatalyst and enhanced visible light photocatalytic activity. *RSC Adv.* **2017**, *7*, 8688–8693. [CrossRef]

44. Nihal Rattan, S.; Manpreet Anjali Harjot Kumar, S.; Sharma, M.; Tripathi, S.K.; Goswamy, J.K. Synthesis and characterization of Ag metal doped SnO2, WO3 and WO$_3$–SnO$_2$ for propan-2-ol sensing. *Results Mater.* **2021**, *9*, 100127. [CrossRef]

45. Nihal Sharma, R.; Sharma, M.; Goswamy, J.K. Au decorated WO$_3$-SnO$_2$ nanocomposite for enhanced benzene vapors sensing performance. *Phys. Scr.* **2023**, *98*, 045809. [CrossRef]

46. Xu, J.; Zhang, L.; Shi, R.; Zhu, Y. Chemical exfoliation of graphitic carbon nitride for efficient heterogeneous photocatalysis. *J. Mater. Chem. A* **2013**, *1*, 14766. [CrossRef]

47. Phan, D.-T.; Chung, G.-S. Reliability of hydrogen sensing based on bimetallic Ni–Pd/graphene composites. *Int. J. Hydrogen Energy* **2014**, *39*, 20294–20304. [CrossRef]

48. Zhang, D.; Sun, Y.; Jiang, C.; Zhang, Y. Room temperature hydrogen gas sensor based on palladium decorated tin oxide/molybdenum disulfide ternary hybrid via hydrothermal route. *Sens. Actuators B Chem.* **2017**, *242*, 15–24. [CrossRef]

49. Ibrahim, A.; Memon, U.B.; Duttagupta, S.P.; Mahesh, I.; Raman, R.K.S.; Sarkar, A.; Pendharkar, G.; Tatiparti, S.S.V. Nano-structured palladium impregnate graphitic carbon nitride composite for efficient hydrogen gas sensing. *Int. J. Hydrogen Energy* **2020**, *45*, 10623–10636. [CrossRef]

50. Saruhan, B.; Lontio Fomekong, R.; Nahirniak, S. Review: Influences of Semiconductor Metal Oxide Properties on Gas Sensing Characteristics. *Front. Sens.* **2021**, *2*, 657931. [CrossRef]

51. Wang, Z.; Ali Haidry, A.; Xie, L.; Zavabeti, A.; Li, Z.; Yin, W.; Lontio Fomekong, R.; Saruhan, B. Acetone sensing applications of Ag modified TiO2 porous nanoparticles synthesized via facile hydrothermal method. *Appl. Surf. Sci.* **2020**, *533*, 147383. [CrossRef]

52. Zhang, R.; Wang, Y.; Zhang, Z.; Cao, J. Highly Sensitive Acetone Gas Sensor Based on g-C3N4 Decorated MgFe2O4 Porous Microspheres Composites. *Sensors* **2018**, *18*, 2211. [CrossRef]

53. Sahani, S.; Park, S.J.; Myung, Y.; Pham, T.-H.; Tung, T.T.; Kim, T. Enhanced Room-Temperature Ethanol Detection by Quasi 2D Nanosheets of an Exfoliated Polymeric Graphitized Carbon Nitride Composite-Based Patterned Sensor. *ACS Omega* **2022**, *7*, 41905–41914. [CrossRef]

54. Malik, R.; Tomer, V.K.; Chaudhary, V.; Dahiya, M.S.; Nehra, S.P.; Duhan, S.; Kailasam, K. A low temperature, highly sensitive and fast response toluene gas sensor based on In(III)-SnO2 loaded cubic mesoporous graphitic carbon nitride. *Sens. Actuators B Chem.* **2018**, *255*, 3564–3575. [CrossRef]

55. Absalan, S.; Nasresfahani, S.h.; Sheikhi, M.H. High-performance carbon monoxide gas sensor based on palladium/tin oxide/porous graphitic carbon nitride nanocomposite. *J. Alloy. Compd.* **2019**, *795*, 79–90. [CrossRef]

56. Nihal Sharma, R.; Kaur, N.; Sharma, M.; Choudhary, B.C.; Goswamy, J.K. Improved room temperature ethanol vapors sensing using silver nanoparticles decorated graphitic carbon nitride (Ag-gCN) nanocomposite. *Mater. Lett.* **2023**, *342*, 134343. [CrossRef]